Palaeogeography, Palaeoclimatology, Palaeoecology 308 (2011) 151–159

Contents lists available at ScienceDirect

Palaeogeography, Palaeoclimatology, Palaeoecology

journal homepage: www.elsevier.com/locate/palaeo

Molecular records of microbialites following the end-Permian mass extinction in Chongyang, Hubei Province, South China

Lin Chen [a], Yongbiao Wang [a], Shucheng Xie [b,*], Stephen Kershaw [c], Man Dong [d], Hao Yang [b], Hao Liu [b], Thomas J. Algeo [e]

[a] State Key Laboratory of Geological Processes and Mineral Resources, China University of Geosciences, Wuhan 430074, PR China
[b] Key Laboratory of Biogeology and Environmental Geology of Ministry of Education, China University of Geosciences, Wuhan 430074, PR China
[c] Institute for the Environment, Brunel University, Kingston Lane, Uxbridge, Middlesex, UB8 3PH, United Kingdom
[d] Research Center of Paleontology and Stratigraphy, Jilin University, Changchun 130026, PR China
[e] Department of Geology, University of Cincinnati, Cincinnati, Ohio 45221-0013, OH, USA

ARTICLE INFO

Article history:
Received 8 December 2009
Received in revised form 21 August 2010
Accepted 14 September 2010
Available online 18 September 2010

Keywords:
Microbialite
Biomarker
Permian–Triassic boundary
Biotic crisis
Chongyang

ABSTRACT

By using gas chromatograph (GC) and GC–mass spectrometry, a series of biomarkers were identified in the aliphatic fractions of extracts from microbialites following the end-Permian faunal mass extinction in Chongyang section, Hubei Province, South China. The dominance of lower-molecular-weight *n*-alkanes in the samples from the section suggests that algae and bacteria were the dominant contributors to the organic fraction preserved in this marine section, with bacteria particularly enhanced within the stromatolite. The end-Permian biotic crisis coincided with a short-term suppression of autotrophs, indicated by the ratio of pristane (Pr) and phytane (Ph) to C_{17} and C_{18} *n*-alkanes, and proliferation of heterotrophs, shown by the ratio of branched-to-normal C_{17} alkanes. The biotic crisis also may have been associated with a transient oxygenation event in the shallow marine, indicated by elevated Pr/Ph ratios and lowered C_{27} 18α(H)-22,29,30-Trisnorneohopane (Ts) to C_{27} 17α(H)-22,29,30-Trisnorhopane (Tm) and gammacerane (γ) to C_{31} homohopane (C_{31}HP) ratios. Subsequently, three short-term episodes of intensified anoxia or enhanced salinity at Chongyang are recorded by decreases in Pr/Ph ratios in conjunction with lithological boundaries in the section.

1. Introduction

The mass extinction just prior to the Permian–Triassic boundary (PTB) was the most severe biotic crisis of the Phanerozoic, with the loss of more than 90% marine species and 70% of terrestrial vertebrate families (Erwin, 1994; Benton and Twitchett, 2003; Bambach et al., 2004). The cause of the extinction is still highly debated. Eruption of the Siberian Traps volcanism, sea-level change, meteorite impact, global oceanic anoxia, and massive methane hydrate release have all been cited as potential causes (Krull and Retallack, 2000; Becker et al., 2001; Wignall, 2001; Benton and Twitchett, 2003; Wignall et al., 2009). Marine biodiversity is generally greatest in shallow-marine facies, especially reef ecosystems. During the end-Permian mass extinction event, shallow-marine faunas suffered an abrupt decline in biodiversity, and tropical reef ecosystems were among the most severely affected (Wang et al., 2005), leading to a global gap in reef facies (James, 1983; Kiessling, 2001; Weidlich et al., 2003) and the widespread occurrence of microbialites throughout the ~5-Myr-long Early Triassic (Lehrmann et al., 2006; Mundil et al., 2010).

Microbialites are the fossilized remains of various microbes that favored the trapping and binding of sediments (Burne and Moore, 1987; Kershaw et al., 2007). These rocks were widely distributed in the Precambrian and early Palaeozoic but decrease sharply in abundance during the Ordovician, but the reasons for this decline are unclear. It may be due to the evolutionary radiation of metazoans (Golonka, 2002; Sheehan and Harris, 2004), although Riding (1992) emphasized the importance of carbonate saturation of seawater as a major driver of microbial calcification. Significantly, microbialites resurged during some of the biotic crises of the Phanerozoic, such as that of the Early Ordovician (Adachi, et al., 2009), Late Ordovician (Sheehan and Harris, 2004), Late Devonian F/F extinction(Stephens and Sumner, 2003; Adachi and Ezaki, 2007, but see Feng et al., 2010, showing decline of calcimicrobies after the F/F), and Early Triassic (Schubert and Bottjer, 1992; Lehrmann et al., 2003; Baud et al., 2007; Pruss et al., 2007). Early Triassic microbialites, which proliferated following the end-Permian mass extinction, have been reported from numerous regions (Flügel and Kiessling, 2002; Wang et al., 2005), including Iran, Turkey, Hungary, Mexico, Poland, the Transcaucasus, Japan, and South China. However, in western North America the

* Corresponding author. Tel./fax: +86 27 67885096.
E-mail address: xiecug@163.com (S. Xie).

0031-0182/$ – see front matter © 2010 Elsevier B.V. All rights reserved.
doi:10.1016/j.palaeo.2010.09.010

earliest microbialites are in the later part of the Early Triassic. Whether the proliferation of microbialites was due to a paucity of metazoans following the mass extinction event or to the persistence and/or recurrence of hostile environmental conditions during the Early Triassic has not been determined yet. Investigations of the microbialite record are thus needed in order to determine patterns of co-evolution of organisms and Earth-surface environments during these critical periods.

Previous studies of microbialites have focused on their sedimentary characteristics, which were studied mainly using microscopic techniques (Kershaw et al., 1999, 2002; Ezaki et al., 2003; Crasquin-Soleau and Kershaw, 2005; Yang et al., 2006; Kershaw et al., 2007; Wu et al., 2007a,b; Jiang et al., 2008; Wang et al., 2009) and isotopic measurements of carbon (Krull et al., 2004; Wang et al., 2007; Mu et al., 2009; Wang et al., 2009), strontium (Wang et al., 2007), and iron (Blanckenburg et al., 2008). To date, little work has been conducted on geolipids, in particular biomarkers preserved in the microbialites (Maliński et al., 2009). A number of recent investigations have demonstrated the potential utility of biomarkers for paleoenvironmental analysis of PTB sections (Grice et al., 2005a,b; Sephton et al., 2005; Xie et al., 2005; Huang et al., 2007; Wang, 2007; Wang and Visscher, 2007; Xie et al., 2007a,b; Ruan et al., 2008; Cao et al., 2009), suggesting that the molecular records preserved in contemporaneous microbialites may provide additional insight concerning the causes of the end-Permian biotic crisis. Here, we examine the molecular records of PTB microbialites in Chongyang, Hubei Province, South China (Fig. 1), in order to assess the relationship of microbial ecosystem development to changing marine environmental conditions during and following the end-Permian biotic crisis.

2. Sample site and methods

2.1. Sample site

The outcrops of PTB strata in the Chongyang section, Hubei Province, South China, are well-exposed and the end-Permian mass extinction horizon is easily identified (Fig. 2). The lowermost 4.0 m of the section consists of bioclastic limestones of the Changhsing Formation, which contains a diverse and abundant fossil assemblage, including calcareous algae, fusulinids, foraminifers, bryozoans, crinoids, brachiopods, and other metazoans, and represent deposition in a shallow, normal-marine environment. The presence of *Palaeofusulina* in this unit demonstrates a Late Permian age. The overlying 7.5 m of section consists of sparsely fossiliferous microbialites (Fig. 2). The conodont fossils *Hindeodus parvus*, *H. typicalis* and *H. latidentatus* (Yin et al., 2001) were found about 6.6 m above the base of this unit, demonstrating that the upper part of the microbialite is of earliest Triassic (early Griesbachian) age (Yang et al., 2006). The uppermost 4.5 m of the section consists of oolitic limestone and non-fossiliferous calcareous mudstone (Fig. 2). Altogether 33 samples were collected for lipid analysis, with 23 taken from the microbialite unit.

In the Chongyang section, the structure of the microbialites shows an obvious change from thrombolitic character in the lower part of the section (0–180 cm) to stromatolitic character higher up (180–750 cm). The thrombolites have a typical clotted structure (Fig. 2a) and are composed of varied arrangements of centimeter-sized sparitic clots associated with a few microgastropods, bivalves and ostracodes (Fig. 3a,b). On the other hand, the stromatolites show a typical layered fabric (Fig. 2b) featuring an alternation of dark-colored laminae containing a higher concentration of calcified microbes, and light-colored laminae dominated by detrital carbonate minerals. Microgastropods, bivalves, and ostracods are rare in lamellar microbialites. Calcified coccoid structures, typically 20–30 μm in size and interpreted here as cyanobacterial remains, are usually preserved along the margins of light-colored microbialite or micrite layers (Fig. 3c,d).

2.2. Experimental methods

After cleaning the surface, the air-dried samples were ground to less than 80 mesh. As much as 100 g of each sample was Soxhlet-extracted with chloroform for 72 h with native copper added to

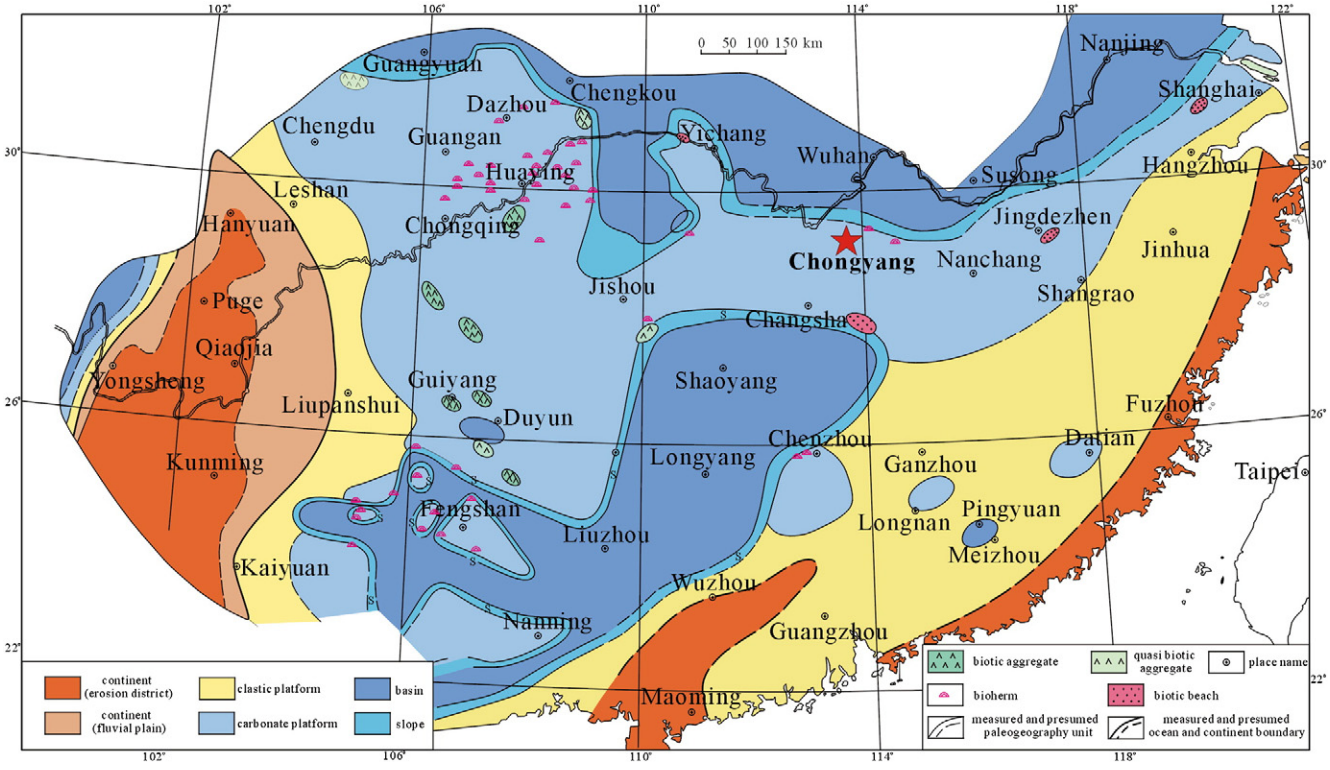

Fig. 1. Geography and location of the Chongyang section, Hubei Province, South China (modified after Feng et al., 1996).

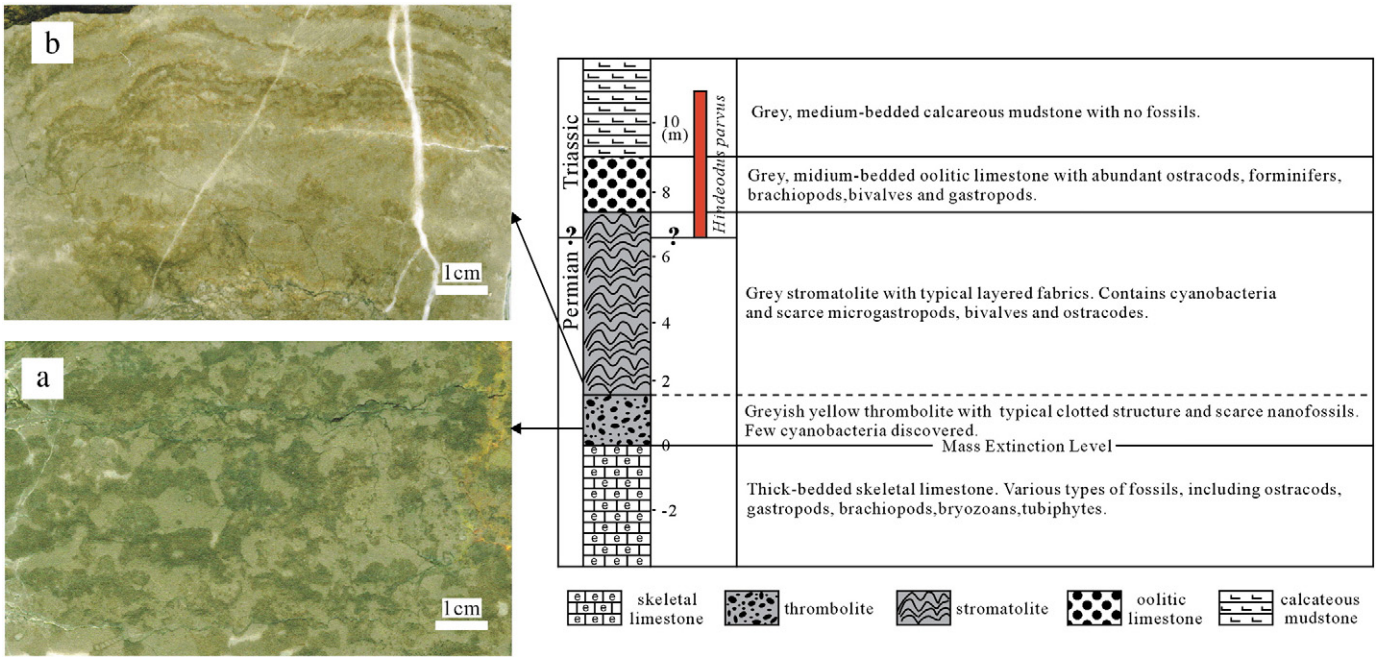

Fig. 2. Lithology of the Chongyang section. Note that sample elevations are given relative to the end-Permian mass extinction horizon. The images show polished sections of thrombolite and stromatolite in Chongyang section, exhibiting an occurrence of clotted fabric (a: 50–65 cm), and layered structures (b: 190–202 cm).

remove natural sulfur. The extract was then concentrated on a rotary evaporator under reduced pressure and transferred to a small vial. Following evaporation of the remaining solvent, the total extractable lipid was weighed. The asphaltenes in the extracts were eliminated by precipitation in hexane. The hexane-solute organics were fractionated by column chromatography (filled with silica gel 60) into saturated hydrocarbons, aromatics and non-hydrocarbons, by sequential elution with hexane, benzene and alcohol, respectively.

A blank sample was analyzed to monitor for contamination. To avoid laboratory contamination, the glassware used was rinsed with distilled water, and then annealed at 500 °C for 10 h. Before using, all the glassware was rinsed with dichloromethane (DCM). The gloves

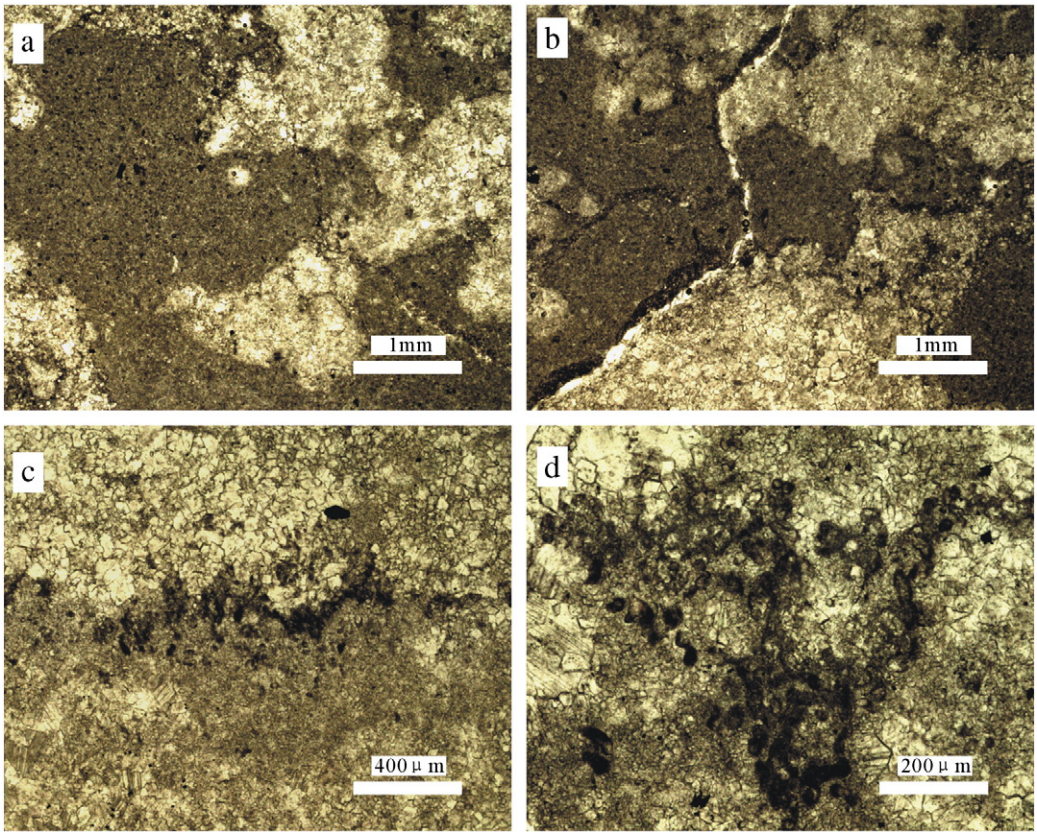

Fig. 3. Microstructures of thrombolites (a, b: 50–65 cm) and stromatolites (c, d: 190–202 cm) from Chongyang section under a light microscope.

and filter paper used in the experiment were Soxhlet-extracted with DCM for 72 h prior to use.

The alkane fractions were first analyzed by using a Shimadzu GC-2010 gas chromatograph equipped with a flame ionization detector (FID) and a ZB-1 fused silica capillary column (60 m × 0.25 mm × 0.25 μm). The FID temperature was set at 320 °C and the injector at 300 °C in the splitless mode. The GC oven temperature was programmed from 70 to 300 at 3 °C/min, and finally to hold at 300 °C for 20 min. Nitrogen was used as carrier gas. GC–MS analysis of the alkane fractions was conducted on a Hewlett-Packard 5973A MS, interfaced directly with a Hewlett-Packard 6890 GC equipped with an DB-5MS fused silica capillary column (60 m × 0.25 mm × 0.25 μm). The operating conditions were as follows: temperature ramped from 70 to 300 °C at 3 °C/min, finally held at 300 °C for 40 min, helium was used as carrier gas; the ionization energy of the mass spectrometer was set at 70 eV; the scan range was from 50 to 550 m/z. The quantification was conducted by calculating the peak area of the ion chromatograms or the GC–MS total ion current of the target compounds.

3. Results and discussion

3.1. Distribution of hydrocarbons

The distributions of *n*-alkanes in selected samples from the Chongyang section are shown in Fig. 4. The *n*-alkanes are present over the range from *n*-C_{14} to *n*-C_{35}. They show an invariant, monomodal distribution in the *n*-alkane carbon number, with the dominant homologues being *n*-C_{17} or *n*-C_{18}, indicative of the dominant contribution of microorganisms.

Along with the *n*-alkanes, some monomethyl branched alkanes, such as 2-methyl and 3-methyl alkanes, were found in the samples. There are also some isoprenoid hydrocarbons, including pristane and phytane. The pristane/phytane (Pr/Ph) ratio ranges from 0.68 to 1.35 through the section.

The m/z 191 mass chromatograms are shown in Fig. 5. They revealed the distribution of long-chain tricyclic terpanes, triterpanes in selected samples from the Chongyang section. C_{19} to C_{29} tricyclic terpanes, 17α(H), 21β(H) and 17β(H), 21α(H) hopanes, C_{27} 18α(H)-22,29,30-Trisnorneohopane (Ts), C_{27} 17α(H)-22,29,30-Trisnorhopane(Tm), and gammacerane (γ) are present. The 17α(H), 21β(H) and 17β(H), 21α(H) hopanes are represented by C_{29} to C_{35} homologues, and 17α(H), 21β(H) hopanes are the most abundant hopanoids, with the C_{30} homologue as the dominant compound.

Steranes identified are mainly C_{27} to C_{29} regular steranes, with typical m/z 217 mass chromatograms being shown in Fig. 5. All the samples from the Chongyang section are dominated by C_{27} homologues.

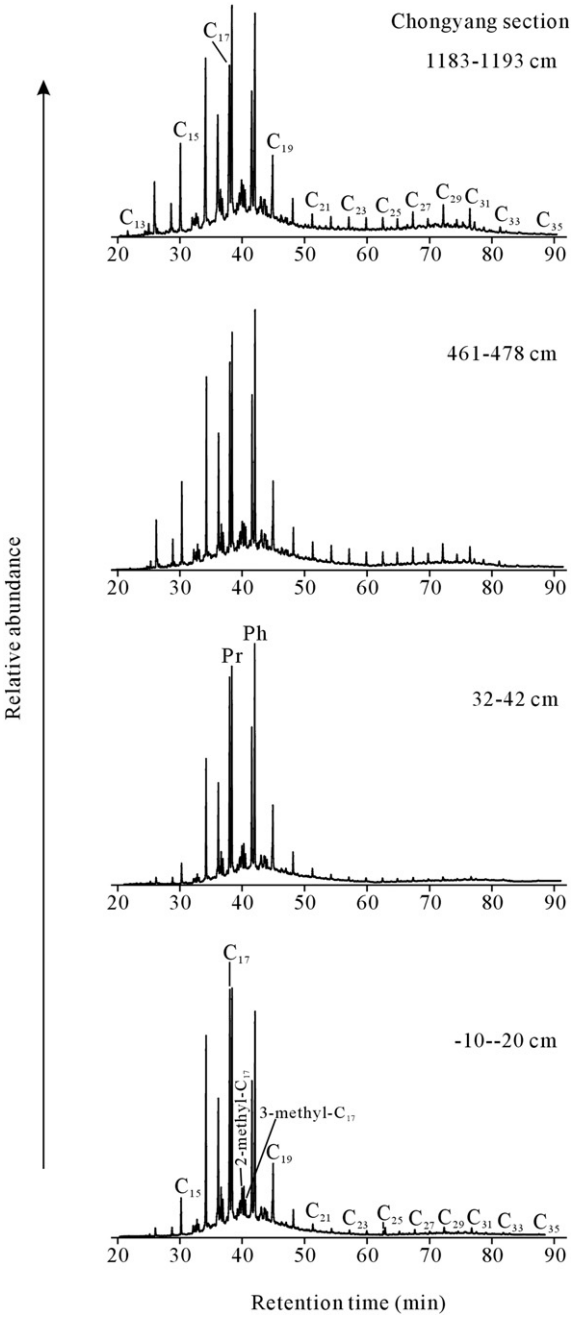

Fig. 4. Gas chromatograms showing alkane distributions of selected samples from the Chongyang section.

3.2. Molecular evidence for microbial changes

3.2.1. Relative abundance of bacteria and algae

All samples from the Chongyang section show a monomodal distribution in the *n*-alkane carbon number. The dominance of lower-molecular-weight *n*-alkanes suggests that the main organic input was from algae and bacteria. The ratio of hopanes (total amount of C_{29} to C_{34} hopanes) to steranes (total amount of C_{27} to C_{29} regular steranes) has been proposed to reflect the change in the abundance of bacteria relative to algae in the marine ecosystem (Peters et al., 2005). Three stratigraphic intervals of differing hopane-to-sterane ratios are evident in the Chongyang section (Fig. 6). High values are found within the stromatolitic microbialite interval, indicative of a relatively high abundance of bacteria. In contrast, both the skeletal limestones and thrombolites that underlie the stromatolitic interval and the oolitic limestones and calcareous mudstones that overlie it show lower values, indicative of algal dominance. It is surprising to note that no obvious changes in hopane-to-sterane ratios occurred at the end-Permian mass extinction horizon, implying that the relative abundances of bacteria and algae were unchanged during this event in this section. In contrast, a dramatic change is observed at the contact between the thrombolitic and stromatolitic microbialites, following the mass extinction event.

3.2.2. Relative abundance of autotrophs and heterotrophs

Pristane and phytane have been demonstrated to be derived primarily from autotrophs within marine ecosystems, originating from the oxidation or reduction of the phytol side chain of chlorophyll (Didyk et al., 1978; Rontani and Volkman, 2003). The total abundance of pristane and phytane relative to the amount of C_{17} and C_{18} *n*-alkanes, expressed by the ratio of (Pr + Ph)/(*n*-C_{17} + *n*-C_{18}) calculated from the total ion current, is thus indicative of variation in the relative

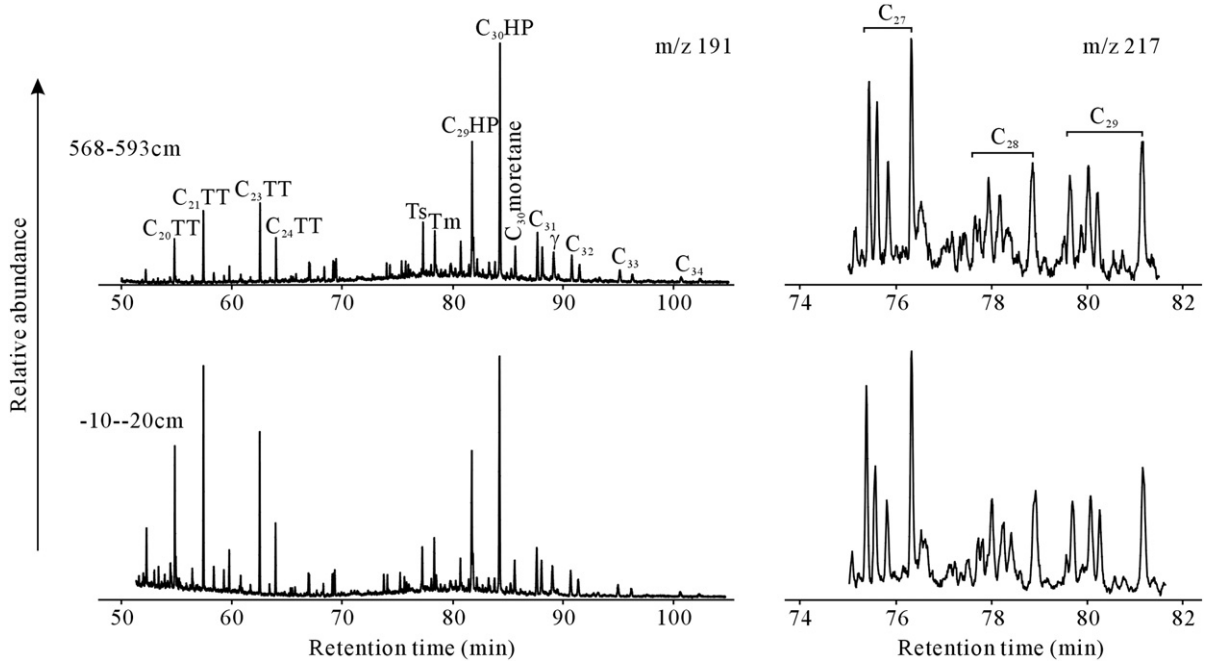

Fig. 5. Representative m/z 191, m/z 217 mass chromatograms of alkanes for samples −10 to −20 cm and 568 to 593 cm from the Chongyang section.

contributions of autotrophs and heterotrophs to the organic fraction of the sediment. This biomarker ratio fluctuates strongly throughout the section, although within a fairly narrow range of values (1.20–1.60; Fig. 6). The most sustained (i.e., multisample) decrease in this ratio occurs across the end-Permian mass extinction horizon, suggesting a decline of autotrophs relative to heterotrophs in conjunction with this event. The inferred decline of autotrophs may have been the consequence of changes in oceanic chemistry harmful to autotrophs (e.g., Fraiser and Bottjer, 2007; Knoll et al., 2007), but another possibility is an increase in cloud cover that prohibited photosynthesis (e.g., Beerling et al., 2007). If representative of biomass changes during the end-Permian crisis, then the decline in autotrophs may have resulted in reduced energy flows to higher trophic levels (cf. Payne and van de Schootbrugge, 2007), leading to at least short-term general starvation within PTB marine ecosystems.

The maxima of the ratio of $(Pr+Ph)/(n\text{-}C_{17}+n\text{-}C_{18})$ are found within the stromatolitic part of the microbialite unit, suggesting that favorable conditions for autotrophs existed during this period. Kershaw et al. (1999) suggested that microbialite carbonate crusts may have been associated with the development of CO_2-rich waters on the South China platform. Extending this argument, it is possible that elevated CO_2 levels triggered elevated rates of photosynthesis among some autotrophs such as cyanobacteria (e.g., Canfield and Des Marais, 1993; Wieland et al., 2008), leading to increased ratios of $(Pr+Ph)/(n\text{-}C_{17}+n\text{-}C_{18})$. These factors could account for the short-term decrease and succeeding long-term increase in this biomarker

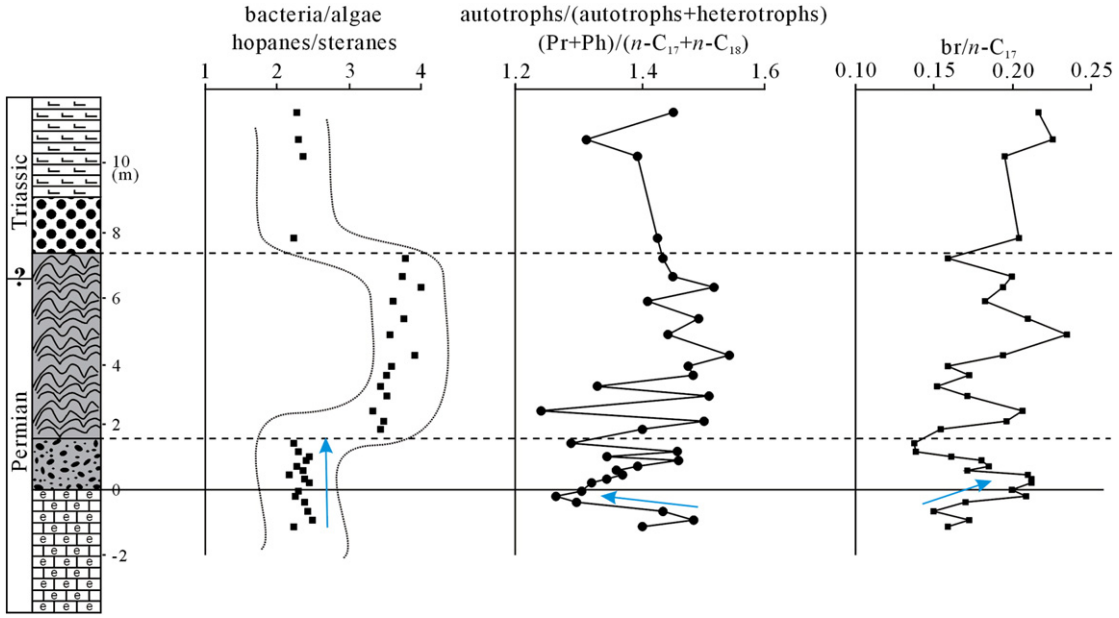

Fig. 6. The profiles of the ratios of hopanes/steranes, $(Pr+Ph)/(n\text{-}C_{17}+n\text{-}C_{18})$ and (2-methyl + 3-methyl C_{17})/n-C_{17} (br/n-C_{17}) in the Chongyang section. The dotted lines show general variation trends of the hopane–sterane ratio across the section. See Fig. 2 for lithologic key.

ratio observed in the Chongyang section (Fig. 6). Volcanism could have exerted a transient detrimental effect via deposition of toxic gases and ash and a sustained stimulatory effect via CO_2 emissions (Xie et al., 2010). Whether or not this biomarker record is the product of a large-scale volcanic eruption awaits further investigation.

The ratio of branched-to-normal alkanes, expressed here by 2-methyl and 3-methyl to normal C_{17} alkanes, fluctuates throughout the section (Fig. 6). This pattern may be indicative of frequent changes within the microbial ecosystem, including within the microbialite interval. Monomethyl branched alkanes are mainly related to the contribution of bacteria. Sulfate-reducing bacteria produce some 2-methyl and 3-methyl fatty acids and ethers, and these compounds can be converted to 2-methyl and 3-methyl monomethyl alkanes (Peckmann et al., 2004). The ratio of branched-to-normal alkanes may reflect variation in the composition of the microbial community, especially among heterotrophs. The end-Permian mass extinction horizon is associated with an increase in the ratio of branched-to-normal alkanes, coincident with the previously noted decline in the $(Pr+Ph)/(n\text{-}C_{17}+n\text{-}C_{18})$ ratio. The opposing trends of these two biomarker proxies across the mass extinction horizon indicate that the decline among autotrophs and increase among heterotrophs occurred concurrently. Both trends commence ~50 cm below the mass extinction horizon, suggesting that ecosystem changes were underway well in advance of the crash represented by the extinction event itself.

3.3. Molecular fingerprints of sedimentary environmental conditions

3.3.1. Pr/Ph

The nature of the sedimentary environment, especially with regard to bottomwater redox conditions, is one of the most important factors affecting the preservation of organic matter. Pristane and phytane are molecules derived primarily from the chlorophyll side chain phytol (Rontani and Volkman, 2003), and their relative abundance in the sediment is influenced by bottomwater redox conditions and salinity at the time of deposition (Didyk et al., 1978; Hughes et al., 1995). Reducing conditions are commonly inferred on the basis of Pr/Ph ratios that are either <0.6 (Peters and Moldowan, 1993) or <1.0 (Hughes et al., 1995; Peters et al., 2005). In addition, anoxia could be associated with hypersaline conditions, and lower Pr/Ph ratio might be related to the enhanced marine salinity if associated with the enhanced abundance of gammacerane.

All the samples analysed for the Chongyang section show Pr/Ph ratios greater than 0.6, ranging from 0.68 to 1.35, with lower values being found mainly in the upper part of the section (above 400 cm) (Fig. 7). These values suggest that the shallow-marine environment of the Chongyang section did not experience severe anoxia during the end-Permian extinction event, and that even the overlying Lower Triassic part of the section experienced only moderately reducing conditions. However, a decline in Pr/Ph ratios is observed to occur in conjunction with each of three lithologic contacts, i.e., those between (1) skeletal limestone and thrombolite, (2) thrombolite and stromatolite, and (3) stromatolite and oolitic limestone. Owing to the observed considerable variation in Pr/Ph ratios within each interval of uniform lithology, it is inferred that these drops are not related to lithologic changes in the study section but, rather, due to episodic shifts toward more reducing conditions in the depositional system.

The observation that the lowest Pr/Ph ratio in the study section (0.68) is in the oolitic limestone above the microbialite interval (Fig. 7) is unexpected, because ooids form through turbulence at very shallow (few meters) water depths in modern Bahamas. Ooid formation here may have been linked to processes related to the PTB event, such as mixing of bicarbonate-rich deepwaters into the surface mixed layer of the ocean (cf. Knoll et al., 1996; Nielsen and Shen, 2004; Pruss et al., 2006), which could have led to a concurrent shift toward more reducing conditions, as implied by low Pr/Ph ratios. Alternatively, the declined Pr/Ph ratio might be contributed by the enhanced salinity during the oolitic limestone deposition. This would be in case in consideration of its association with the elevated abundance of gammacerane as shown below by the γ/C_{31}HP index.

3.3.2. Ts/Tm and γ/C_{31}HP index

The relative abundances of the hopane compounds C_{27} 17α(H)-22,29,30-Trisnorhopane (Tm) and C_{27} 18α(H)-22,29,30-Trisnorneohopane (Ts) are commonly influenced by bottomwater redox conditions, with higher Ts/Tm ratios under more reducing conditions (Moldowan et al., 1986; Peters et al., 2005). However, Ts/Tm is also known to vary as a function of organic source and/or thermal maturity (Moldowan et al., 1986), requiring caution in its use as a redox proxy. Gammacerane (γ) is a non-hopanoid C_{30} triterpane probably derived from tetrahymanol (Sinninghe Damsté et al., 1995), and often present in samples from hypersaline marine and nonmarine depositional environments. Relatively high abundances of gammacerane (expressed by the γ/C_{31}HP index, i.e., the ratio of gammacerane to C_{31} hopanes) are typically interpreted as evidence of a stratified,

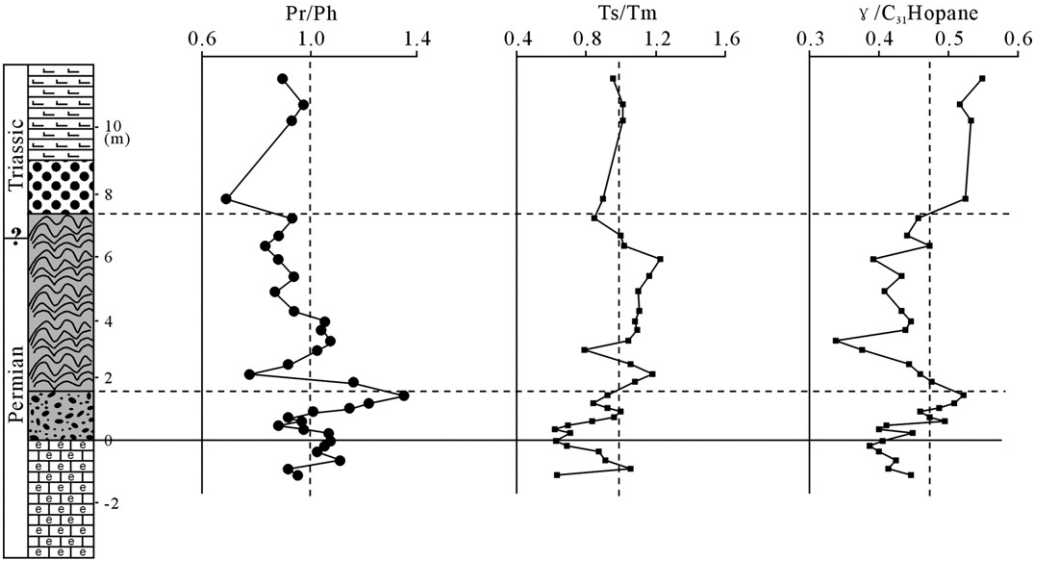

Fig. 7. Profiles showing trends of the ratios of Pr/Ph, Ts/Tm, γ/C_{31}HP in the Chongyang section. See Fig. 2 for lithologic key.

anoxic water column, which can be associated with hypersaline conditions (Schoell et al., 1994; Kenig et al., 1995; Sinninghe Damsté et al., 1995).

Both of these biomarker ratios fluctuate considerably within the Chongyang section, possibly indicating substantial redox variation (Fig. 7). A general trend toward higher values upsection, particularly in the γ/C_{31}HP index, supports the shift toward more reducing conditions in the Early Triassic inferred from Pr/Ph ratios (see Section 3.3.1). Low values of Ts/Tm and γ/C_{31}HP at the end-Permian extinction horizon are consistent with high values of the Pr/Ph ratio, indicating transient development of more oxidizing conditions. A geologically short interval of relatively oxidizing conditions just above the mass extinction horizon has been inferred in other studies also. For example, sulphur isotope data in pelagic black shales in Japan are consistent with such an oxygenation event (Kajiwara et al., 1994), and narrow oxygenated intervals have been reported from the Mazzin member at Bulla, Italy (Twitchett and Wignall, 1996). Thus, our biomolecular proxy data may provide evidence that this short-term oxygenation event had a broad geographic range and occurred in shallow cratonic as well as open-ocean settings.

Some of the high-frequency stratigraphic variation in these proxies is likely controlled by non-redox influences; however, both Ts/Tm and γ/C_{31}HP ratios appear to show changes related to lithologic variations in the upper part of the section. For example, the stromatolite unit is characterized by higher Ts/Tm and lower γ/C_{31}HP ratios, whereas the overlying oolitic limestone and calcareous mudstone units are characterized by lower Ts/Tm and higher γ/C_{31}HP ratios. Furthermore, these two biomarker ratios tend to show significant changes at or near lithologic contacts. These observations suggest that the Ts/Tm and γ/C_{31}HP ratios may record both redox and non-redox influences such as salinity changes.

3.3.3. General implications for redox variability

Despite agreement regarding a general shift toward more reducing conditions upward within the Chongyang section, the molecular redox proxies discussed above frequently yield inconsistent redox interpretations over short stratigraphic intervals, e.g., within the upper half of the thrombolite. One of the difficulties in interpreting redox proxies in the PTB interval is that redox conditions may have varied at geologically short timescales. This pattern is especially characteristic of some shallow-marine sections, which were subjected to repeated, brief episodes of upwelling of anoxic deep waters (Algeo et al., 2007). Such high-frequency variation can lead to "mixed" redox signals because some proxies rapidly acquire a euxinic signature whereas others do not (Algeo et al., submitted for publication). For example, the presence of any measurable amount of aryl isoprenoids, which are produced by green sulfur bacteria in a single growth season, provide evidence of photic-zone euxinia (Summons and Powell, 1987; Hays et al., 2007), whereas sulfidization of reactive sedimentary Fe (utilized in redox proxies such as Fe_{HR}/Fe_T and DOP) can require significantly longer periods of time (Canfield et al., 1992; Raiswell and Canfield, 1998). In the context of the present study, it should be noted that little is known at present about differences in the characteristic timescales required by various biomarkers to acquire a specific redox signature, an area that will require further investigation in order to substantiate the significance of biomarkers as redox proxies. Influence of other factors such as marine salinity further complicates the redox interpretation of biomarker records.

3.4. Microbial–environmental relationships at the PTB

The biomarker data of this study document strong relationships between changes in environmental conditions and microbial ecosystem development at Chongyang. The Chongyang shallow-marine shelf was subjected to multiple environmental perturbations, most notably at the level of the end-Permian extinction event (correlative with the skeletal limestone-microbialite contact), but also at the contacts of the thrombolite–stromatolite and stromatolite–oolitic limestone units (Fig. 2). These perturbations included strong fluctuations in environmental conditions, including a transient oxygenation event at the mass extinction horizon, followed by a series of reducing events or enhanced salinity that coincided with major facies transitions (Fig. 6). Concurrently, large changes in energy flows within the Chongyang marine ecosystem took place, as reflected in a decrease in autotroph abundance at the mass extinction horizon followed by large fluctuations in autotroph-to-heterotroph ratios within the microbialite interval (Fig. 7). Controls on the transition from thrombolite to stromatolite growth within the microbialite unit (Fig. 2) are uncertain but possibly related to changes in microbial ecosystem composition, as reflected in variations in heterotroph abundance (Fig. 7). We conclude that the sustained development of microbial communities in the immediate aftermath of the end-Permian crisis at Chongyang was due to environmentally unstable conditions that were either episodically or persistently hostile to metazoan life.

4. Conclusions

A variety of biomarkers, including C_{14}-C_{35} *n*-alkanes, branched monomethyl alkanes, pristane, phytane, C_{19}–C_{29} tricyclic terpanes, C_{29}–C_{34} triterpanes and C_{27}–C_{29} regular steranes, were identified in substantial amounts in an Upper Permian to Lower Triassic carbonate succession containing microbialites at Chongyang in South China. The dominance of lower-molecular-weight *n*-alkanes is indicative of the dominant contribution of algae and bacteria to the organic fraction of this section. As shown by elevated ratios of hopanes to steranes, the stromatolitic microbialite interval is marked by an enhanced abundance of bacteria to algae, whereas other lithofacies units (i.e., skeletal limestone, thrombolitic microbialite, oolitic limestone, and calcareous mudstone) are dominated by algae. A suppression of autotrophs relative to heterotrophs, indicated by the ratio Pr and Ph to C_{17} and C_{18} *n*-alkanes, and an increase of heterotrophs shown by the ratio of branched-to-normal C_{17} alkanes, were documented across the lithologic contact between the skeletal limestone and thrombolitic microbialite, coincident with the end-Permian faunal mass extinction event.

The Pr/Ph ratio, together with Ts/Tm and γ/C_{31}HP was used to infer sedimentary environmental conditions in the depositional system, although these proxies might be related to lithologic controls in some horizons. Decreases in Pr/Ph ratios across lithologic contacts in the study section may be related to intensification of reducing conditions in association with the enhanced salinity. The lithologic contact between the skeletal limestone and thrombolitic microbialite, which is correlative with the end-Permian biotic crisis, is characterised by elevated Pr/Ph ratios (>1.0) and reduced Ts/Tm and γ/C_{31}HP ratios, suggesting the occurrence of a short-term local oxygenation event in conjunction with the main extinction event in this shallow-marine section.

Acknowledgments

We thank Dr. Margaret L. Fraiser and two anonymous reviewers for constructive and helpful reviews of this manuscript. This work was supported by the 973 project (grant no. 2011CB808800), the National Natural Science Foundation of China (grant nos. 40730209 and 40921062), and the 111 project (B08030). This paper is a contribution to IGCP Project 572.

References

Adachi, N., Ezaki, Y., 2007. Microbial impacts on the genesis of Lower Devonian reefal limestones, eastern Australia. Palaeoworld 16, 301–310.

Adachi, N., Ezaki, Y., Liu, J.B., Cao, J., 2009. Early Ordovician reef construction in Anhui Province, South China: a geobiological transition from microbial-to metazoan-dominant reefs. Sedimentary Geology 220, 1–11.

Algeo, T.J., Ellwood, B.B., Nguyen, T.K.T., Rowe, H., Maynard, J.B., 2007. The Permian–Triassic boundary at Nhi Tao, Vietnam: evidence for recurrent influx of sulfidic watermasses to a shallow-marine carbonate platform. Palaeogeography, Palaeoclimatology, Palaeoecology 252, 304–327.

Algeo, T., Henderson, C., Ellwood, B., Rowe, H., Elswick, E., Bates, S., Lyons, T., Hower, J.C., Smith, C., Maynard, J.B., Hays, L., Summons, R., Fulton, J., Freeman, K., submitted for publication. Elevated sediment fluxes in the Sverdrup Basin prior to the end-Permian mass extinction: link to Siberian Traps volcanism? Geological Society of America Bulletin.

Bambach, R.K., Knoll, A.H., Wang, S.C., 2004. Origination, extinction, and mass depletions of marine diversity. Paleobiology 30, 522–542.

Baud, A., Richoz, S., Pruss, S., 2007. The lower Triassic anachronistic carbonate facies in space and time. Global and Planetary Change 55, 81–89.

Becker, L., Poreda, R.J., Hunt, A.G., Bunch, T.E., Rampino, M., 2001. Impact event at the Permian–Triassic boundary: evidence from extraterrestrial noble gases in fullerenes. Science 291, 1530–1533.

Beerling, D.J., Harfoot, M., Lomax, B., Pyle, J.A., 2007. The stability of the stratospheric ozone layer during the end-Permian eruption of the Siberian Traps. Philosophical Transactions of the Royal Society of London. Series A 365, 1843–1866.

Benton, M.J., Twitchett, R.J., 2003. How to kill (almost) all life: the end-Permian extinction event. Trends in Ecology & Evolution 18, 358–365.

Blanckenburg, F.V., Mamberti, M., Schoenberg, R., Kamber, B.S., Webb, G.E., 2008. The iron isotope composition of microbial carbonate. Chemical Geology 249, 113–128.

Burne, R.V., Moore, L.S., 1987. Microbialites: organosedimentary deposits of benthic microbial communities. Palaios 2, 241–254.

Canfield, D.E., Des Marais, D.J., 1993. Biogeochemical cycles of carbon, sulfur, and free oxygen in a microbial mat. Geochimica et Cosmochimica Acta 57, 3971–3984.

Canfield, D.E., Raiswell, R., Bottrell, S., 1992. The reactivity of sedimentary iron minerals toward sulfide. American Journal of Science 292, 659–683.

Cao, C.Q., Love, G.D., Hays, L.E., Wang, W., Shen, S.Z., Summons, R.E., 2009. Biogeochemical evidence for euxinic oceans and ecological disturbance presaging the end-Permian mass extinction event. Earth and Planetary Science Letters 281, 188–201.

Crasquin-Soleau, S., Kershaw, S., 2005. Ostracod fauna from the Permian–Triassic boundary interval of South China (Huaying Mountains, eastern Sichuan Province): palaeoenvironmental significance. Palaeogeography, Palaeoclimatology, Palaeoecology 217, 131–141.

Didyk, B.M., Simoneit, B.R.T., Brassell, S.C., Eglinton, G., 1978. Organic geochemical indicators of palaeoenvironmental conditions of sedimentation. Nature 272, 216–222.

Erwin, D.H., 1994. The Permo-Triassic extinction. Nature 367, 231–236.

Ezaki, Y., Liu, J.B., Adachi, N., 2003. Earliest Triassic microbialite micro- to megastructures in the Huaying area of Sichuan Province, South China: implications for the nature of oceanic conditions after the end-Permian extinction. Palaios 18, 388–402.

Feng, Z.Z., Yang, Y.Q., Jin, Z.K., He, Y.B., Wu, S.H., Xin, W.J., Bao, Z.D., Tan, J., 1996. Permian lithofacies palaeogeography in South China. Acta Sedimentologica Sinica 14, 1–11 (in Chinese).

Feng, Q., Gong, Y.-M., Riding, R., 2010. Mid-Late Devonian calcified marine algae and cyanobacteria, south China. Journal of Paleontology 84, 569–587.

Flügel, E., Kiessling, W., 2002. Patterns of Phanerozoic reef crises. In: Kiessling, W., Flügel, E., Golonka, J. (Eds.), Phanerozoic reef patterns: Society for Sedimentary Geology Special Publication, 72, pp. 691–733.

Fraiser, L.M., Bottjer, D.J., 2007. Elevated atmospheric CO_2 and the delayed biotic recovery from the end-Permian mass extinction. Palaeogeography, Palaeoclimatology, Palaeoecology 252, 164–175.

Golonka, J., 2002. Plate-tectonic maps of the Phanerozoic. In: Kiessling, W., Flügel, E., Golonka, J. (Eds.), Phanerozoic reef patterns: Society for Sedimentary Geology Special Publication, 72, pp. 21–75.

Grice, K., Cao, C., Love, G.D., Böttcher, M.E., Twitchett, R.J., Grosjean, E., Summons, R.E., Turgeon, S.C., Dunning, W., Jin, Y., 2005a. Photic zone euxinia during the Permian–Triassic superanoxic event. Science 307, 706–709.

Grice, K., Twitchett, R., Alexander, R., Foster, C.B., Looy, C.V., Greenwood, P., 2005b. A potential biomarker for the Permian–Triassic ecological crisis. Earth and Planetary Science Letters 236, 315–321.

Hays, L.E., Beatty, T., Henderson, C.M., Love, G.D., Summons, R.E., 2007. Evidence for photic zone euxinia through the end-Permian mass extinction in the Panthalassic Ocean (Peace River Basin, Western Canada). Paleaoworld 16, 39–50.

Huang, X.Y., Jiao, D., Lu, L.Q., Xie, S.C., Huang, J.H., Wang, Y.B., Yin, H.F., Wang, H.M., Zhang, K.X., Lai, X.L., 2007. The fluctuating environment associated with the episodic biotic crisis during the Permo/Triassic transition: evidence from microbial biomarkers in Changxing, Zhejiang Province. Science in China Series D: Earth Science 50, 1052–1059.

Hughes, W.B., Holba, A.G., Dzou, L.I.P., 1995. The ratios of dibenzothiophene to phenanthrene and pristane to phytane as indicators of depositional environment and lithology of petroleum source rocks. Geochimica et Cosmochimica Acta 59, 3581–3598.

James, N.P., 1983. Reef environment. In: Scholle, P.A., Bebout, D.G., Moore, C.H. (Eds.), Carbonate depositional environments: American Association of Petroleum Geologists Memoir, 33, pp. 346–440.

Jiang, H.X., Wu, Y.S., Cai, C.F., 2008. Filamentous cyanobacteria fossils and their significance in the Permian–Triassic boundary section at Laolongdong, Chongqing. Chinese Science Bulletin 53, 1871–1879.

Kajiwara, Y., Yamakita, S., Ishida, K., Ishiga, H., Imai, A., 1994. Development of a largely anoxic stratified ocean and its temporary massive mixing at the Permian/Triassic boundary supported by the sulfur isotopic record. Palaeogeography, Palaeoclimatology, Palaeoecology 111, 367–379.

Kenig, F., Sinninghe Damsté, J.S., Frewin, N.L., Hayes, J.M., de Leeuw, J.W., 1995. Molecular indicators for paleoenvironmental change in a Messinian evaporitic sequence (Vena del Gesso, Italy). II. High-resolution variations in abundances and ^{13}C contents of free and sulphur-bound carbon skeletons in a single marl bed. Organic Geochemistry 23, 485–526.

Kershaw, S., Zhang, T.S., Lan, G.Z., 1999. A ?microbialite carbonate crust at the Permian–Triassic boundary in South China, and its palaeoenvironmental significance. Palaeogeography, Palaeoclimatology, Palaeoecology 146, 1–18.

Kershaw, S., Guo, L., Swift, A., Fan, J.S., 2002. ?Microbialites in the Permian–Triassic boundary interval in central China: structure, age and distribution. Facies 47, 83–90.

Kershaw, S., Li, Y., Crasquin-Soleau, S., Feng, Q.L., Mu, X.N., Collin, P.Y., Reynolds, A., Guo, L., 2007. Earliest Triassic microbialites in the South China block and other areas: controls on their growth and distribution. Facies 53, 409–425.

Kiessling, W., 2001. Paleoclimatic significance of Phanerozoic reefs. Geology 29, 751–754.

Knoll, A.H., Bambach, R.K., Canfield, D.E., Grotzinger, J.P., 1996. Comparative Earth history and Late Permian mass extinction. Science 273, 452–457.

Knoll, A.H., Bambach, R.K., Payne, J.L., Pruss, S., Fischer, W.W., 2007. Paleophysiology and end-Permian mass extinction. Earth and Planetary Science Letters 256, 295–313.

Krull, E.S., Retallack, G.J., 2000. $\delta^{13}C$ depth profiles from paleosols across the Permian–Triassic boundary: evidence for methane release. Geological Society of America Bulletin 112, 1459–1472.

Krull, E.S., Lehrmann, D.J., Druke, D., Kessel, B., Yu, Y.Y., Li, R.X., 2004. Stable carbon isotope stratigraphy across the Permian–Triassic boundary in shallow marine carbonate platforms, Nanpanjiang Basin, south China. Palaeogeography, Palaeoclimatology, Palaeoecology 204, 297–315.

Lehrmann, D.J., Payne, J.L., Felix, S.V., 2003. Permian–Triassic boundary sections from shallow-marine carbonate platforms of the Nanpanjiang Basin, south China: implications for oceanic conditions associated with the end-Permian extinction and its aftermath. Palaios 18, 138–152.

Lehrmann, D.J., Ramezani, J., Bowring, S.A., Martin, M.W., Montgomery, P., Enos, P., Payne, J.L., Orchard, M.J., Wang, H., Wei, J., 2006. Timing of recovery from the end-Permian extinction: geochronologic and biostratigraphic constraints from south China. Geology 34, 1053–1056.

Maliński, E., Gasiewicz, A., Witkowski, A., Szafranek, J., Pihlaja, K., Oksman, P., Wiinamäki, K., 2009. Biomarker features of sabkha-associated microbialites Dolomite (Upper Permian) of northern Poland. Palaeogeography, Palaeoclimatology, Palaeoecology 273, 92–101.

Moldowan, J.M., Sundararaman, P., Schoell, M., 1986. Sensitivity of biomarker properties to depositional environment and/or source input in the Lower Toarcian of SW-Germany. Organic Geochemistry 10, 915–926.

Mu, X.N., Kershaw, S., Li, Y., Guo, L., Qi, Y.P., Reynolds, A., 2009. High-resolution carbon isotope changes in the Permian–Triassic boundary interval, Chongqing, South China; implications for control and growth of earliest Triassic microbialites. Journal of Asian Earth Sciences 36, 434–441.

Mundil, R., Pálfy, J., Renne, P.R., Brack, P., 2010. The Triassic time scale: new constraints and a review of geochronological data. In: Lucas, S.G. (Ed.), The Triassic timescale: Geological Society of London, Special Publication, 334, pp. 41–60.

Nielsen, J.K., Shen, Y., 2004. Evidence for sulfidic deep water during the Late Permian in the East Greenland Basin. Geology 32, 1037–1040.

Payne, J., van de Schootbrugge, B., 2007. Life in Triassic oceans: links between benthic and planktonic recovery and radiation. In: Falkowski, P.G., Knoll, A.H. (Eds.), The Evolution of Primary Producers in the Sea. Academic Press, New York, pp. 165–189.

Peckmann, J., Thiel, V., Reitner, J., Taviani, M., Aharon, P., Michaelis, W., 2004. A microbial mat of a large sulfur bacterium preserved in a Miocene methane-seep limestone. Geomicrobiology Journal 21, 247–255.

Peters, K.E., Moldowan, J.M., 1993. The Biomarker Guide: Interpreting Molecular Fossils in Petroleum and Ancient Sediments. Prentice Hall, Englewood Cliffs, New Jersey.

Peters, K.E., Walters, C.C., Moldowan, J.M., 2005. The Biomarker Guide. Cambridge University Press, Cambridge, UK.

Pruss, S.B., Bottjer, D.J., Corsetti, F.A., Baud, A., 2006. A global marine sedimentary response to the end-Permian mass extinction: examples from southern Turkey and the western United States. Earth Science Reviews 78, 193–206.

Pruss, S.B., Payne, J.L., Bottjer, D.J., 2007. *Placunopsis* bioherms: the first metazoan buildups following the end-Permian mass extinction. Palaios 22, 17–23.

Raiswell, R., Canfield, D.E., 1998. Sources of iron for pyrite formation in marine sediments. American Journal of Science 298, 219–245.

Riding, R., 1992. Temporal variation in calcification in marine cyanobacteria. Journal of the Geological Society 149, 979–989.

Rontani, J.F., Volkman, J.K., 2003. Phytol degradation products as biogeochemical tracers in aquatic environments. Organic Geochemistry 34, 1–35.

Ruan, X.Y., Luo, G.M., Hu, S.Z., Chen, F., Sun, S., Wu, W.J., Guo, Q.Z., Liu, G.Q., 2008. Molecular records of primary producers and sedimentary environmental conditions of Late Permian rocks in Northeast Sichuan, China. Journal of the China University of Geosciences 19, 471–480.

Schoell, M., Hwang, R.J., Carlson, R.M.K., Welton, J.E., 1994. Carbon isotopic compositions of individual biomarkers in gilsonites (Utah). Organic Geochemistry 21, 673–683.

Schubert, J.K., Bottjer, D.J., 1992. Early Triassic stromatolites as post-mass extinction disaster forms. Geology 20, 883–886.

Sephton, M.A., Looy, C.V., Brinkhuis, H., Wignall, P.B., de Leeuw, J.W., Visscher, H., 2005. Catastrophic soil erosion during the end-Permian biotic crisis. Geology 33, 941–944.

Sheehan, P.M., Harris, M.T., 2004. Microbialite resurgence after the Late Ordovician extinction. Nature 430, 75–78.

Sinninghe Damsté, J.S., Kenig, F., Koopmans, M.P., Koster, J., Schouten, S., Hayes, J.M., de Leeuw, J.W., 1995. Evidence for gammacerane as an indicator of water column stratification. Geochimica et Cosmochimica Acta 59, 1895–1900.

Stephens, N.P., Sumner, D.Y., 2003. Famennian microbial reef facies, Napier and Oscar Ranges, Canning Basin, western Australia. Sedimentology 50, 1283–1302.

Summons, R.E., Powell, T.G., 1987. Identification of aryl isoprenoids in source rocks and crude oils: biological markers for the green sulphur bacteria. Geochimica et Cosmochimica Acta 51, 557–566.

Twitchett, R.J., Wignall, P.B., 1996. Trace fossils and the aftermath of the Permo-Triassic mass extinction: evidence from northern Italy. Palaeogeography, Palaeoclimatology, Palaeoecology 124, 137–151.

Wang, C.J., 2007. Anomalous hopane distributions at the Permian–Triassic boundary, Meishan, China—evidence for the end-Permian marine ecosystem collapse. Organic Geochemistry 38, 52–66.

Wang, C.J., Visscher, H., 2007. Abundance anomalies of aromatic biomarkers in the Permian–Triassic boundary section at Meishan, China—evidence of end-Permian terrestrial ecosystem collapse. Palaeogeography, Palaeoclimatology, Palaeoecology 252, 291–303.

Wang, Y.B., Tong, J.N., Wang, J.S., Zhou, X.G., 2005. Calcimicrobialite after end-Permian mass extinction in South China and its palaeoenvironmental significance. Chinese Science Bulletin 50, 665–671.

Wang, W., Kano, A., Okumura, T., Ma, Y.S., Matsumoto, R., Matsuda, N., Ueno, K., Chen, X.Z., Kakuwa, Y., Gharaie, M.H.M., Ilkhchi, M.R., 2007. Isotopic chemostratigraphy of the microbialite-bearing Permian–Triassic boundary section in the Zagros Mountains, Iran. Chemical Geology 244, 708–714.

Wang, Q.X., Tong, J.N., Song, H.J., Yang, H., 2009. Ecological evolution across the Permian/Triassic boundary at the Kangjiaping Section in Cili County, Hunan Province, China. Science in China Series D: Earth Science 52, 797–806.

Weidlich, O., Kiessling, W., Flügel, E., 2003. Permian–Triassic boundary interval as a model for forcing marine ecosystem collapse by long-term atmospheric oxygen drop. Geology 31, 961–964.

Wieland, A., Pape, T., Möbius, J., Klock, J.-H., Michaelis, W., 2008. Carbon pools and isotopic trends in a hypersaline cyanobacterial mat. Geobiology 6, 171–186.

Wignall, P.B., 2001. Large igneous provinces and mass extinctions. Earth Science Reviews 53, 1–33.

Wignall, P.B., Sun, Y.D., Bond, D.P.G., Izon, G., Newton, R.J., Védrine, S., Widdowson, M., Ali, J.R., Lai, X.L., Jiang, H.S., Cope, H., Bottrell, S.H., 2009. Volcanism, mass extinction, and carbon isotope fluctuations in the Middle Permian of China. Science 324, 1179–1182.

Wu, Y.S., Fan, J.S., Jiang, H.X., Yang, W., 2007a. Extinction pattern of reef ecosystems in latest Permian. Chinese Science Bulletin 52, 512–520.

Wu, Y.S., Jiang, H.X., Yang, W., Fan, J.S., 2007b. Microbialite of anoxic condition from Permian–Triassic transition in Guizhou, China. Science in China Series D: Earth Science 50, 1040–1051.

Xie, S., Pancost, R.D., Yin, H., Wang, H., Evershed, R.P., 2005. Two episodes of microbial change coupled with Permo/Triassic faunal mass extinction. Nature 434, 494–497.

Xie, S.C., Pancost, R.D., Huang, J.H., Wignall, P.B., Yu, J.X., Tang, X.Y., Chen, L., Huang, X.Y., Lai, X.L., 2007a. Changes in the global carbon cycle occurred as two episodes during the Permian–Triassic crisis. Geology 35, 1083–1086.

Xie, S.C., Pancost, R.D., Huang, X.Y., Jiao, D., Lu, L.Q., Huang, J.H., Yang, F.Q., Evershed, R.P., 2007b. Molecular and isotopic evidence for episodic environmental change across the Permo/Triassic boundary at Meishan in South China. Global and Planetary Change 55, 56–65.

Xie, S.C., Pancost, R.D., Wang, Y.B., Yang, H., Wignall, P.B., Luo, G.M., Jia, C.L., Chen, L., 2010. Cyanobacterial blooms tied to volcanism during the 5 m.y. Permo-Triassic biotic crisis. Geology 38, 447–450.

Yang, H., Zhang, S.X., Jiang, H.S., Wang, Y.B., 2006. Age and general characteristics of the calimicrobialite near the Permian–Triassic boundary in Chongyang, Hubei Province. Journal of the China University of Geosciences 17, 121–125.

Yin, H., Zhang, K., Tong, J., Yang, Z., Wu, S., 2001. The global stratotype section and point (GSSP) of the Permian–Triassic boundary. Episodes 24, 102–114.